Paper:UK00106 *revised version*

Running head: Methanol Electro-oxidation of Ternary Electrocatalyst

Title: Performance of Ternary PtRuRh/C Electrocatalyst with Varying Pt:Ru:Rh Ratio for Methanol Electro-oxidation

Authors: Tomoyuki Kawaguchi, Yasuhiro Rachi, Wataru Sugimoto, Yasushi Murakami and Yoshio Takasu*

Affiliations: Department of Fine Materials Engineering, Faculty of Textile Science and Technology, Shinshu University

Address: 3-15-1 Tokida, Ueda 386-8567, Japan

Tel: +81-268-21-5451

Fax: +81-268-22-9048

E-mail: ytakasu@shinshu-u.ac.jp

Abstract

Highly dispersed ternary PtRuRh/C anode catalysts for direct methanol fuel cells were prepared with various contents and their electro-catalytic activities towards methanol oxidation at 25 and 60 °C were examined to investigate the influence of the catalyst composition. Electrocatalysts were prepared by a co-impregnation method using ethanolic solutions of metal precursors and carbon black followed by pyrolysis under reducing conditions. X-ray diffraction analysis revealed that the fcc peaks shifted to higher diffraction angles with increasing Rh content, indicating the alloying of Rh into the fcc structure. In terms of the mass specific current density, the activity towards methanol oxidation differed significantly depending on the catalysts composition and cell temperature. The catalyst prepared at a ratio of Pt:Ru:Rh = 1:1:2 exhibited the highest activity at 60 °C of 155 A $(g\text{-}Pt)^{-1}$ at 0.5 V vs. RHE.

Key words: Direct methanol fuel cell, Anode catalyst, PtRuRh, Methanol electrooxidation

1. Introduction

Platinum-based alloy nanoparticles have been extensively studied as anode catalysts in low-temperature fuel cells, such as polymer electrolyte fuel cells using CO-containing hydrogen or methanol as fuel. Direct methanol fuel cells (DMFCs), have been a subject of intense research because of their numerous advantages [1]. Since Pt is readily poisoned by CO, an intermediate produced during methanol oxidation, the design and synthesis of Pt-based binary alloy catalysts that inhibit CO-poisoning is one of the major challenges. Examples of these materials are PtRu [2-15], PtSn [16-31], PtMo [32-34], PtRh [19,35], PtRe [19,25]. The PtRu alloy is presently considered as one of the most promising materials [7]. The enhancement in activity has been attributed to both the bi-functional nature of the alloy surface and electronic effects resulting from electron transfer from the promoter element to the d-band of Pt.

Studies on more complicated systems, such as ternary and quaternary metals, have also been conducted. It has been reported that addition of W [18,41], Sn [18], Os [40], Pd [41], Ag [42], Au [40,42], Rh [42] to PtRu provides improved CO tolerance. PtRuOs [43,44], PtRuMo [18,45], PtRuW [18,46], PtRuNi [47], PtRuRh [48], PtRuSn [18,49], PtRuAu [49], PtRuOsIr [43], PtRuMoW [50] and PtRuRhNi [51] were investigated as highly active catalysts for the methanol oxidation reaction. Despite these extensive efforts, factors such as structure-property relations are still not well understood. For example, the optimal

composition of the alloy catalyst could vary depending on the operating temperature [52-56]. Therefore, a systematic evaluation of catalysts with various compositions at different operation temperatures is required. In this work, we selected Rh as the third metal. Rh has the same fcc structure as Pt and the Rh is known to form a solid solution [57]. Previous studies on PtRh and PtRuRh have shown that Rh can enhance the catalytic activity towards CO and methanol oxidation [48].

Here, we report the preparation, structure and catalytic performance of ternary PtRuRh/C catalysts. PtRuRh/C catalysts with 13 different alloy composition were prepared. The structure was carefully characterized and the composition-activity relation towards the methanol oxidation at 25 and 60 °C was evaluated.

2. Experimental

PtRuRh/C catalysts with 13 different metal ratios were prepared by a conventional co-impregnation method [8]. The nominal contents, presented by mass% and mol%, and metal loading amount are summarized in Table 1. The metal ratios of these PtRuRh/C catalysts are shown in a triangle graph (Fig. 1), where the numbers in the parentheses mean the molar ratio of Pt, Ru and Rh. All catalysts were prepared by introducing carbon black (Vulcan XC-72R) into a mixture of $Pt(NH_3)_2(NO_2)_2$, $Ru(NO_3)_3$ and $Rh(NO_3)_3$ dissolved in ethanol. 4 mM (M = mol dm^{-3}) ethanolic solutions of the compounds were used as metal sources. After thorough mixing the precursor solution was dried at 60 °C to a powder. The dried powder was then reduced in a tube furnace under flowing H_2(10%)+N_2(90%) gas for 2 h at 200 °C. The structure of the catalysts was characterized by X-ray diffraction (XRD, Rigaku RINT-2550 with monochromated CuK_α radiation at 40 kV and 50 mA) and high-resolution scanning electron microscopy (HR-SEM, Hitachi S-5000). XRD profiles in the 2θ range of 15 – 95° were scanned at a scanning speed of 2° min^{-1}. Detailed profiles in the 2θ range of 62 – 75° were examined with a step scan of 0.02° and counting time of 5 s. Electrochemical studies were conducted using a three-electrode type beaker cell equipped with a platinum mesh counter electrode, an Ag/AgCl reference electrode and the working electrode. A Luggin capillary faced the working electrode at a distance of 2 mm. The working electrodes were prepared by the thin film electrode method [58,59]. Briefly, 20 mg of the catalyst powder was

dispersed in 10 mL of methanol and was subject to ultrasonification for 30 min. Then, 20 μL of the catalyst powder dispersion (40 μg of the catalyst powder) was dropped on a polished Glassy Carbon (Tokai Carbon Co., Ltd.) substrate (grade 20SS, 5 mm in diameter). After drying at 60 °C, 20 μL of a 1 wt% Nafion® alcoholic solution was further dropped on the electrode surface to stabilize the electrocatalysts to the Glassy Carbon rod surface and heated again at 60 °C. All electrode potentials will be referred to the RHE(*t*) scale corrected for the temperature effect. The electrocatalytic oxidation of methanol was studied by chronoamperometry in 1 M CH_3OH + 0.5 M H_2SO_4 solution. The currents after 1800 s were used as the quasi-steady state current. Electrochemical measurements were carried out at 25 and 60 °C.

3. Results and discussion

HR-SEM observation and XRD analysis showed that highly-dispersed alloy particles on the carbon support were obtained. In a comparative study using metal chlorides as metal sources (H_2PtCl_6, $RuCl_6$ and $RhCl_3$), we found that the dispersion state and particle size distribution were not as good as the nitrate-based system. Thus, choice of the metal source is a critical factor in the catalyst preparation.

Typical HR-SEM images of selected PtRuRh/C catalysts prepared at different molar ratios are shown in Fig. 2. The HR-SEM image of PtRu/C is also shown for comparison. Uniformly dispersed metal nanoparticles supported on carbon black were obtained for PtRu/C and PtRuRh/C catalysts with negligible agglomeration.

The XRD patterns of the PtRuRh/C catalysts are shown in Fig. 3. All of the XRD peaks could be indexed based on the fcc structure and the shift of the XRD peaks towards high diffraction angles indicate the alloying of Ru and Rh into the fcc structure. For the $Pt_1Ru_2Rh_1$/C and $Pt_1Ru_2Rh_2$/C (g and i in Fig. 3A), a small shoulder peak is evident at 2θ ~ 44º, which may be attributed to Ru metal. Besides these two Ru-rich compositions, it can be said that the catalysts are well alloyed. The fcc lattice parameter *a* of these catalysts are listed in Table 2 assuming that these alloy particles are completely homogeneous. In Fig. 4, the lattice parameter *a* of these PtRuRh/C catalysts composing equimolar ratio of Pt and Ru are plotted against the Rh content. The lattice parameter *a* gradually decreased with an increase in

the Rh content showing that the extent of alloying of these ternary alloy particles are not perfect but considerably well alloyed. Table 2 also presents the crystallite size of these catalysts determined using the Sherrer equation. Since the broadning of the XRD diffaction peaks for alloy catalysts are influenced by both crystallite size and extent of alloying, the significant figures of the crystallite size are single.

Figure 5 shows a few typical steady-state cyclic voltammograms of the PtRuRh/C catalysts in the 0.5 M H_2SO_4 solution at 60 °C. Before the measurement of the methanol oxidation by the chronoamperometry, these catalyst electrodes were pre-treated in the electrolytic solution without methanol by cycling of the electrode potential between 0.05 and 0.8 V vs. RHE at 10 mV s^{-1} for 30 min. The methanol electro-oxidation current densities normalized per unit mass of Pt and PtRu measured at 0.50, 0.45, 0.40 V vs. RHE at 60 °C are shown in Figs. 6 and 7, respectively. Regardless of the potential, the addition of Ru and Rh increases the mass activity towards methanol oxidation. The PtRuRh/C catalyst prepared at a ratio of Pt:Ru:Rh = 1:1:2 exhibited the maximum activity of 155 A $(g\text{-}Pt)^{-1}$ and 102 A $(g\text{-}PtRu)^{-1}$ at 0.50 V vs. RHE. This is an increace of 31 and 1.4 times compared to Pt/C (5 A $(g\text{-}Pt)^{-1}$) and PtRu/C (111 A $(g\text{-}Pt)^{-1}$ or 73 A $(g\text{-}PtRu)^{-1}$), respectively.

The enhanced methanol electro-oxidation for the PtRuRh/C electrocatalyst can be attributed to the change in the electronic properties of Pt, the effect of higher surface area (smaller particles, high dispersion states), and/or particle size of the metal nanoparticles by

addition of the Rh. By comparing activities per surface area of exposed metal, a qualitative comparison of the electrocatalytic activity can be made. The CO stripping voltammetry is a method often employed to estimate the electrochemically active surface area and performance of the CO oxidation reaction of Pt based electrocatalysts [9-13]. In the case of PtRuRh/C electrocatalysts, the CO oxidation behavior was strongly influenced by measurement procedures such as CO adsorption potential, temperature and cycle number etc. Thus, the measurement of the oxidation potential and the electrochemically active surface area by CO stripping with reasonable reliabiliy was difficult for the present ternary catalysts. We have previously reported that the catalytic activity of PtRu/C catalysts per real surface area for the oxidation of methanol increased with an increase in the particle size of PtRu [14]. However, such size effect is not observed in this investigation. That is, the catalytic activities of $Pt_1Ru_1Rh_4$/C and $Pt_1Ru_1Rh_8$/C were lower than those of the other $Pt_1Ru_1Rh_x$/C catalysts, while the crystallite sizes of these catalysts were larger than those of the other catalysts.

The methanol electro-oxidation current densities per total metal mass measured at 0.50, 0.45 and 0.40 V vs. RHE at 60 °C are shown in Fig. 7. When comparing the PtRuRh/C catalysts prepared at a fixed Pt:Ru ratio, for example of Pt:Ru:Rh = 1:1:*x*, $Pt_1Ru_1Rh_{1/2}$/C showed lower mass activity based on the total mass of metal than PtRu/C. However, with increasing Rh content, an increase in activity was observed up to $Pt_1Ru_1Rh_2$/C. Further increase in Rh beyond this composition led to a decrease in activity. The $Pt_1Ru_1Rh_2$/C was the

most active ternary catalyst, exhibiting 60 A (g-PtRuRh)$^{-1}$. However, this catalyst was less active than the Pt_1Ru_1/C catalyst (73 A (g-metal)$^{-1}$). The reason for the lower activity may be the difference in particle size and electrochemically active surface area since the metal loading was slightly higher for $Pt_1Ru_1Rh_2$/C. Such factors are known to influence the overall mass activity[14,15]. More active PtRuRh/C may be prepared by optimizing the particle size, thus the metal surface area, by controlling the composition and the loading.

Methanol electro-oxidation current densities normalized to the mass of Pt and PtRuRh at 25 °C are illustrated in Figs. 9 and 10. The activity per Pt as well as PtRuRh mass tends to be close to or lower than that of PtRu/C catalyst. The addition of Rh is evidently disadvantageous for methanol electro-oxidation at 25 °C. This is a clear difference from the trend observed at 60 °C (Figs. 6-8). The optimal composition for methanol oxidation at 25 °C seems to be situated on the Pt-rich compositions. This may be ascribed to the fact that under such conditions methanol dehydrogenation, which favours on Pt surfaces, is the rate determining step. The electronic effect of additions of Ru and Rh with given composition is expected to contribute to the electrocatalytic activity for methanol oxidation equally independent of the operating temperature. On the other hand, methanol and water adsorption energies should vary with temperature. In the case of binary PtRu, methanol adsorption and dehydrogenation may also occur on Ru sites at elevated temperature [54, 60-64]. The ternary PtRuRh/C system appears to follow the same trend as PtRu, where Ru-rich catalysts were

preferred at elevated temperature, while Pt-rich catalysts were more active at 25 °C.

Another possible reason for the difference in optimal compositions at different temperatures may be the difference in methanol oxidation mechanism. Different pathways of methanol oxidation on Pt in acidic electrolytes via CO, COH, HCOOH and intermediates are known [65]. COH and HCOOH can be further oxidized to adsorbed CO while formic acid undergoes a dual pathway oxidation to CO_2. Such reaction pathways would be expected to vary with operating temperature, catalyst composition and catalyst structure.

4. Conclusions

Well alloyed PtRuRh/C electrocatalysts with 13 different compositions were prepared by a co-impregnation reductive pyrolysis method and their electro-catalytic activity towards methanol electro-oxidation at 25 °C and 60 °C was examined. At 60 °C, the activity towards the methanol oxidation reaction differed significantly depending on the catalysts composition. The catalyst prepared at the ratio of Pt:Ru:Rh = 1:1:2 exhibited the highest Pt utilization with, 155 A $(g\text{-}Pt)^{-1}$. At 25 °C, the effect of Rh addition was disadvantageous and the PtRu/C catalyst without Rh showed the highest activity. The results suggest that the composition of the PtRuRh/C catalyst has a dramatic effect on its electrocatalytic activity. Moreover, the best composition of PtRuRh/C catalysts for methanol oxidation differed depending on the operating temperature.

Acknowledgements

This work was supported in part by the “Polymer Electrolyte Fuel Cell Program” from the New Energy and Industrial Technology Development Organization (NEDO) of Japan, in collaboration with Toray Industries, Inc., and a 21st Century COE Program from MEXT, Japan. The $Pt(NH_3)_2(NO_2)_2$ complex was a gift from Ishihuku Metal Industry Co., Ltd. We gratefully acknowledge their help.

References

[1] S. R. Narayanan and T. I. Valdez, Portable direct methnol fuel cell systems, in Handbook of Fuel Cells Fundamentals Technology and Applications (edited by W. Vielstich, A. Lamm and H. A. Gasteiger), Vol. 4 (John Wiley & Sons Ltd, Chichester, 2003) pp. 1133−1141.

[2] P. Waszcuk, G. – Q. Lu, A. Wiecowski, C. Lu, C. Rice, R. I. Masel, Electrochim. Acta 47 (2002) 3637.

[3] M. Watanabe and S. Motoo, J. Electroanal. Chem. 60 (1975) 267.

[4] T. Iwasita, F. C. Nart and W. Vielstich, Ber. Bunsen-Ges. Phys. Chem. 94 (1990) 1030.

[5] M. Krausa and W. Vielstich, J. Electroanal. Chem. 379 (1994) 307.

[6] Y. Y. Tong, H. S. Kim, P. K. Babu, P. Waszczuk, A. Wieckowski and E. Oldfield, J. Am. Chem. Soc. 124 (2002) 468.

[7] J. O'M. Bockris and H. Wroblowa, J. Electroanal. Chem. 7 (1964) 428.

[8] Y. Takasu, T. Fujiwara, Y. Murakami, M. Oguri, T. Asaki, and W. Sugimoto, J. Electrochem. Soc. 147 (2000) 4421.

[9] H. A. Gasteiger, N. Markovic, P. N. Ross, E. J. Cairns Jr, J. Phys. Chem. 98 (1994) 617.

[10] A. K. Friedrich, K. P. Geyzers, U. Linke, U. Stimming and J. Stumper, J. Electroanal. Chem. 402 (1996) 123.

[11] T. J. Schmidt, M. Noeske, H. A. Gasteiger, R. J. Behm, P. Britz, W. Brijoux and H. Bonnemann, Langmuir 13 (1997) 2591

[12] H. N. Dinh, X. Ren, F. H. Garzon, P. Zelenay and S. Gottesfeld, J. Electroanal. Chem. 491 (2000) 222.

[13] T. Kawaguchi, W. Sugimoto, Y. Murakami, Y. Takasu, Electrochem. Commun. 6 (2004) 480.

[14] Y. Takasu, H. Itaya, T. Iwazaki, R. Miyoshi, T. Ohnuma, W. Sugimoto and Y. Murakami, Chem. Commun. 2001 (2001) 341.

[15] Y. Takasu, W. Sugimoto, and Y. Murakami, Catal. Surv. Asia 7 (2003) 21.

[16] Y. Morimoto, E. B. Yeager, J. Electroanal. Chem. 444 (1998) 95.

[17] T. Frelink, W. Visscher, J. A. R. Van Veen, Surf. Sci. 335 (1995) 353.

[18] M. Gotz, H. Wendt, Electrochim. Acta, 43 (1998) 3637.

[19] D. F. A. Koch, D. A. J. Rand, R. Woods, J. Electroanal. Chem. 70 (1976) 73.

[20] H. W. Lei, S. Suh, B. Gurau, B. Workie, R. Liu, E. S. Smotkin, Electrochim. Acta 47 (2002) 2913.

[21] M. M. P. Janssen, J. Moolhuysen, Electrochim. Acta 21 (1976) 861.

[22] T. Frelink, W. Visscher, J. A. R. van Veen, Electrochim. Acta 39 (1994) 1871.

[23] T. Frelink, W. Visscher, A. P. Cox, J. A. R. van Veen, Electrochim. Acta 40 (1995) 1537.

[24] K. Wang, H. A. Gasteiger, N. M. Markovic, P. N. Ross, Jr, Electrochim. Acta 41 (1996) 2587.

[25] B. Beden, F. Kadirgan, C. Lamy, J. M. Leger, J. Electroanal. Chem. 127 (1981) 75.

[26] M. Shibata, S. Motoo, J. Electroanal. Chem. 209 (1986) 151.

[27] B. Bittins-Cattaneo, T. Iwasita, J. Electroanal. Chem. 238 (1987) 151.

[28] A. S. Aricò, V. Antonucci, Giordano, A. K. Shukla, M. K. Ravikumar, A. Roy, S. Barman D. D. Sarma, J. Power Sources 50 (1994) 295.

[29] G.. Stalnionis, L. Tamašauskaitė-Tamašiūnaitė, V. Pautienienė Z. Jusys, J. Solid State Electrochem. 8 (2004) 900.

[30] A. N. Haner, P. N. Ross, J. Phys Chem. 95 (1991) 3740.

[31] A. K. Shukla, A. S. Aricò, K. M. El-Khatib, H. Kim, P. L. Antonucci and V. Antonucci, Appl. Surf. Sci. 137 (1999) 20.

[32] H. Kita, H. Nalajima, K. Shimizu, J. Electroanal. Chem. 248 (1988) 181.

[33] G. Samjeské, H. Wang, T Löffler, H. Baltruschat, Electrochim. Acta 47 (2002) 3681.

[34] S. Mukerjee, R. C. Urian, Electrochim Acta 47 (2002) 3219.

[35] R. T. S. Oliveira, M. C. Santos, B. G. Marcussi, P. A. P. Nascente, L. O. S. Bulhões, E. C. Pereira, J. Electroanal. Chem 575 (2005) 177.

[36] A. Hamnett, B. J. Kennedy, Electrochim. Acta 33 (1988) 1613.

[37] J. Zeng, J. Y. Lee, J. Power Sources 140 (2005) 268.

[38] T. C. Deivaraj, J. Y. Lee, J. Electrochem. Soc. 151 (2004) A1832.

[39] J. Huang, H. Yang, Q. Huang, Y. Tang, T. Lu, D. L. Akins, J. Electrochem. Soc. 151 (2004) A1810.

[40] C. He, H. R. Kunz, J .M. Fenton, J. Electrochem. Soc. 150 (2003) A1017.

[41] C. He, H. R. Kunz, J .M. Fenton, J. Electrochem. Soc. 144 (1997) 970.

[42] D. R. Venkataraman, H. R. Kunz, J. M. Fenton, J. Electrochem. Soc. 150 (2003) A278.

[43] B. Guau, R. Viswanathan, R. Liu, T. J. Lafrenz, K. L. Ley, E. S. Smotkin, E. Reddington, A. Sapienza, B. C. Chan, T. E. Mallouk, S. Sarangapani, J. Phys. Chem. B 102 (1998) 9997.

[44]K. L. Ley, R. Liu, C. Pu, Q. Fan, N. Leyarovska, C. Segre, E. S. Smotkin, J. Electrochem. Soc. 144 (1997) 1543.

[45] A. Lima, C. Coutanceau, J. M. Leger, C. Lamy, J. Appl. Electrochem. 31 (2001) 379.

[46] M. Umeda, H. Ojima, M. Mohamedi, I. Uchida, J. Power Sources 136 (2004) 10.

[47] K. – W. Park, J. – H. Choi, B. – K. Kwon, S. – A. Lee, Y. – E. Sung, H. – Y. Ha, S. – A.

Hong, H. Kim, A. Wieckowski, J. Phys. Chem. B 106 (2002) 1869.

[48] J. - H. Choi, K. – W. Park, I. – S. Park, W. – H. Nam, Y. – E. Sung, Electrochim. Acta 50 (2004) 787.

[49] A. Aramata, M. Masuda, J. Electrochem. Soc. 138 (1991) 1949.

[50] W. C. Choi, J. D. Kim, S. I. Woo, Catal. Today 74 (2002) 235.

[51] K. – W. Park, J. – H. Choi, S. – A. Lee, C. Pak, H. Chang, Y. – E. Sung, J. Catal. 224 (2004) 236.

[52] A. J. Dickinson, L. P. L. Carrette, J. A. Collins, K. A. Friedrich, U. Stimming, J. Appl. Electrochem. 34 (2004) 975.

[53] X. Ren, P. Zelenay, S. Thomas, J. Davey and S. Gottesfeld, J. Power Sources 86 (2000) 111.

[54] H. A. Gasteiger, N. Markovic, P. N. Ross, Jr, E. J. Cairns, J. Electrochem. Soc. 141 (1994) 1795.

[55] N. Wakabayashi, H. Uchida, M. Watanabe, Electrochem. Solid-State Lett. 5 (2002) E62.

[56] A. S. Aricò, V. Baglio, A. Di Blasi, E. Modica, P. L. Antonucci, V. Antonucci, J. Electroanal. Chem. 557 (2003) 167.

[57]T. B. Massalski, Binary Alloy Phase Diagrams (ASM International, Materials Park, Ohio, 1990)

[58] T. J. Schmidt, M. Noeske, H. A. Gasteiger, R. J. Behm, P. Britz, H. J. Bönnemann, J.

Electrochem. Soc. 145 (1998) 925.

[59] T. J. Schmidt, H. A. Gasteiger, G. D. Stäb, P. M. Urban, D. M. Kolb, R. J. Behm, J. Electrochem. Soc. 145 (1998) 2354.

[60] T. Schultz, S. Zhou and K. Sundmacher, Chem. Eng. Technol. 24 (2001) 1223.

[61] S. Wasmus and A. Küver, J. Electroanal. Chem. 461 (1999) 14.

[62] A.S. Arico, S. Srinivasan and V. Antonucci, Fuel Cells 1 (2001) 133.

[63] K.A. Friedrich, K.P. Geyzers, A.J. Dickinson and U. Stimming, J. Electroanal. Chem. 524–525 (2002) 261.

[64] D. Kardash, C. Korzeniewski and N. Markovic, J. Electroanal. Chem. 500 (2001) 518.

[65] E. A. Batista, H. Hoster, T. Iwasita, J. Electroanal. Chem. 554 (2003) 265.

Figure legends

Fig. 1. Triangle graph showing the content ratios of Pt, Ru and Rh of the PtRuRh/C catalysts prepared in this work.

Fig. 2. HR-SEM images of (a) Pt_1Ru_1/C, (b) $Pt_1Ru_{1/2}Rh_{1/2}/C$, (c) $Pt_1Ru_{1/2}Rh_1/C$, and (d) $Pt_1Ru_1Rh_2/C$.

Fig. 3. The XRD patterns of PtRuRh/C catalyst prepared with different molar ratio of Pt, Ru and Rh. (A) Wide angle profile and (B) detailed measurements near the fcc 220 peak. (a) 1:1:0 (b) 1:1/2:1/2, (c) 1:1/2:1, (d) 1:1:1/2, (e) 1:1:1, (f) 1:1:2, (g) 1:2:1, (h) 1:1:3, (i) 1:2:2, (j) 1:1:4, (k) 1:1:8, (l) 0:0:1.

Fig. 4. The fcc lattice parameter *a* of the $Pt_1Ru_1Rh_x/C$ alloy catalysts against the Rh content, where these alloy particles were assumed to be well homogeneous.

Fig. 5. Typical steady-state cyclic voltammograms of (a) $Pt_1Ru_1Rh_2/C$, (b) $Pt_2Ru_1Rh_1/C$, (c) $Pt_1Ru_2Rh_1/C$, and (d) $Pt_2Ru_1Rh_2/C$ in 0.5 M H_2SO_4 60 °C at 10 mV s^{-1}.

Fig. 6. The mass specific current density per unit mass of Pt measured after 30 min at (a) 0.50, (b) 0.45 and (c) 0.40 V vs. RHE in 0.5 M H_2SO_4 + 1 M CH_3OH at 60 °C.

Fig. 7. The mass specific current density per unit mass of PtRu measured after 30 min at (a) 0.5, (b) 0.45 and (c) 0.4 V vs. RHE in 0.5 M H_2SO_4 + 1 M CH_3OH at 60 °C.

Fig. 8. The mass specific current density per unit mass of PtRuRh measured after 30 min at (a) 0.50, (b) 0.45 and (c) 0.40 V vs. RHE in 0.5 M H_2SO_4 + 1 M CH_3OH at 60 °C.

Fig. 9. The mass specific current density per unit mass of Pt measured after 30 min at (a) 0.50, (b) 0.45 and (c) 0.40 V vs. RHE in 0.5 M H_2SO_4 + 1 M CH_3OH at 25 °C.

Fig. 10. The mass specific current density per unit mass of PtRuRh measured after 30 min at (a) 0.50, (b) 0.45 and (c) 0.40 V vs. RHE in 0.5 M H_2SO_4 + 1 M CH_3OH at 25 °C.

Table 1 The nominal composition of the prepared catalysts.

Sample	Contents / mass%					Contents / mol%		
	Pt	Ru	Rh	Total Metal	Carbon	Pt	Ru	Rh
$Pt_1Ru_{1/5}Rh_{1/5}/C$	21.0	2.18	2.22	25.4	74.6	71.4	14.3	14.3
$Pt_1Ru_{1/5}Rh_{1/2}/C$	20.4	2.11	5.37	27.8	72.2	58.8	11.8	29.4
$Pt_1Ru_{1/2}Rh_2/C$	17.1	4.42	18.0	39.5	60.5	28.6	14.3	57.1
$Pt_1Ru_{1/2}Rh_{1/2}/C$	19.7	5.11	5.20	30.0	70.0	50.0	25.0	25.0
$Pt_1Ru_{1/2}Rh_1/C$	18.8	4.86	9.89	33.6	66.4	40.0	20.0	40.0
$Pt_1Ru_1Rh_{1/2}/C$	18.8	9.73	4.95	33.5	66.5	40.0	40.0	20.0
$Pt_1Ru_1Rh_1/C$	17.9	9.27	9.43	36.6	63.4	33.3	33.3	33.3
$Pt_1Ru_1Rh_2/C$	16.3	8.47	17.2	42.0	58.0	25.0	25.0	50.0
$Pt_1Ru_2Rh_1/C$	16.4	17.0	8.63	42.0	58.0	25.0	50.0	25.0
$Pt_1Ru_1Rh_3/C$	15.1	7.80	23.8	46.7	53.3	20.0	20.0	60.0
$Pt_1Ru_2Rh_2/C$	15.1	15.6	15.9	46.6	53.4	20.0	40.0	40.0
$Pt_1Ru_1Rh_4/C$	13.9	7.22	29.4	50.5	49.5	16.7	16.7	66.7
$Pt_1Ru_1Rh_8/C$	10.8	5.58	45.5	61.9	38.1	10.0	10.0	80.0
Pt_1Ru_1/C	19.8	10.2	–	30.0	70.0	50.0	50.0	–
Pt_1Rh_1/C	19.7	–	10.4	30.1	69.9	50.0	–	50.0
Ru_1Rh_1/C	0	14.9	15.1	30.0	70.0	–	50.0	50.0
Pt/C	30.0	–	–	30.0	70.0	100.0	–	–
Ru/C	0	30.0	–	30.0	70.0	–	100.0	–
Rh/C	–	–	30.0	30.0	70.0	–	–	100.0

Table 2 The lattice parameters and crystallite sizes of the PtRuRh/C catalysts determined from the X-ray diffraction peaks assuming that these ternary alloy particles formed homogeneous alloys.

Pt:Ru:Rh	Rh content / Rh mol%	2θ / °	d / nm	a / Å	Crystallite size / nm
1:1:0	0	68.414	0.13702	3.8755	
1:1:0.5	20	69.05	0.13591	3.8441	2
1:1:1	33.33	69.101	0.13582	3.8416	2
1:1:2	50	69.21	0.13563	3.8362	2
1:1:3	60	69.398	0.13531	3.8271	2
1:1:4	67	69.563	0.13503	3.8192	3
1:1:8	80	69.677	0.13484	3.8139	3
0:0:1	100	69.796	0.13464	3.8082	
1:0.2:0.2	14.29	67.911	0.13791	3.9006	2
1:0.2:0.5	29.41	68.814	0.13632	3.8557	2
1:2:1	25	69.161	0.13572	3.8387	2
1:2:2	40	69.258	0.13555	3.8339	2
1:0.5:0.5	25	68.316	0.13719	3.8803	2
1:0.5:1	40	68.643	0.13661	3.8639	2
1:0.5:2	57.14	68.915	0.13614	3.8506	2

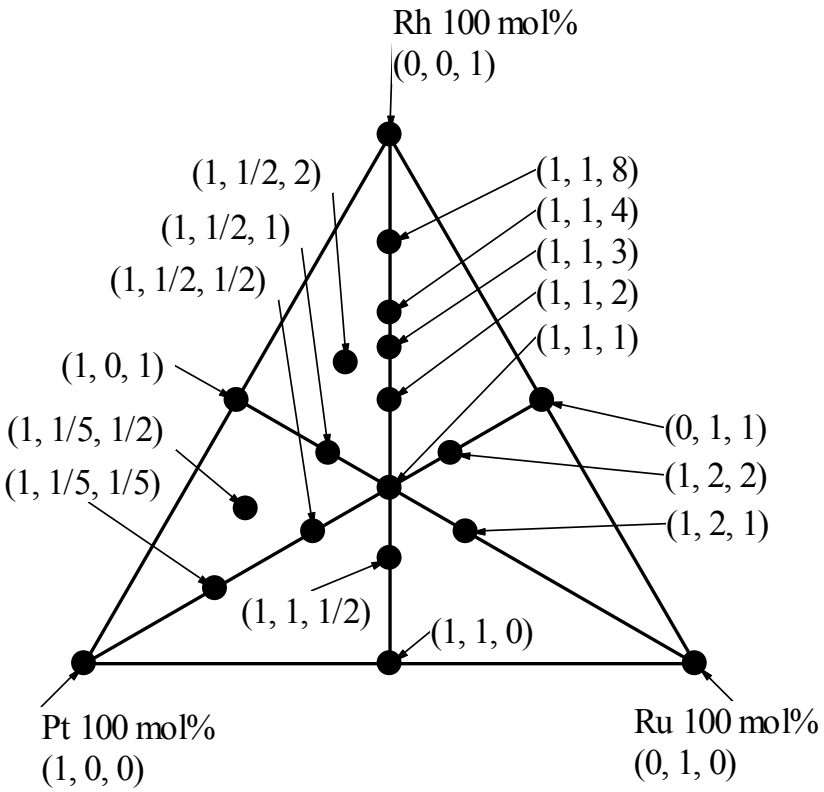

Fig. 1. Triangle graph showing the content ratios of Pt, Ru and Rh of the PtRuRh/C catalysts prepared in this work.

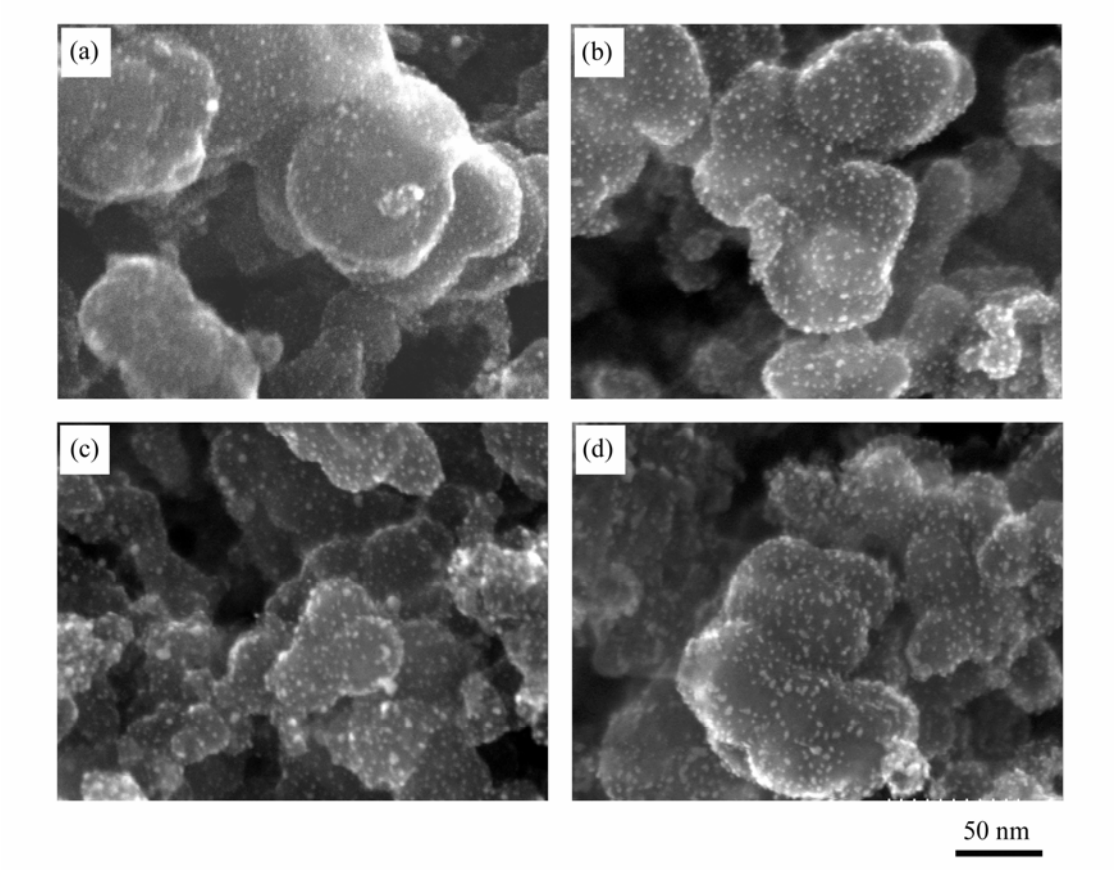

Fig. 2. HR-SEM images of (a) Pt_1Ru_1/C, (b) $Pt_1Ru_{1/2}Rh_{1/2}/C$, (c) $Pt_1Ru_{1/2}Rh_1/C$, and (d) $Pt_1Ru_1Rh_2/C$.

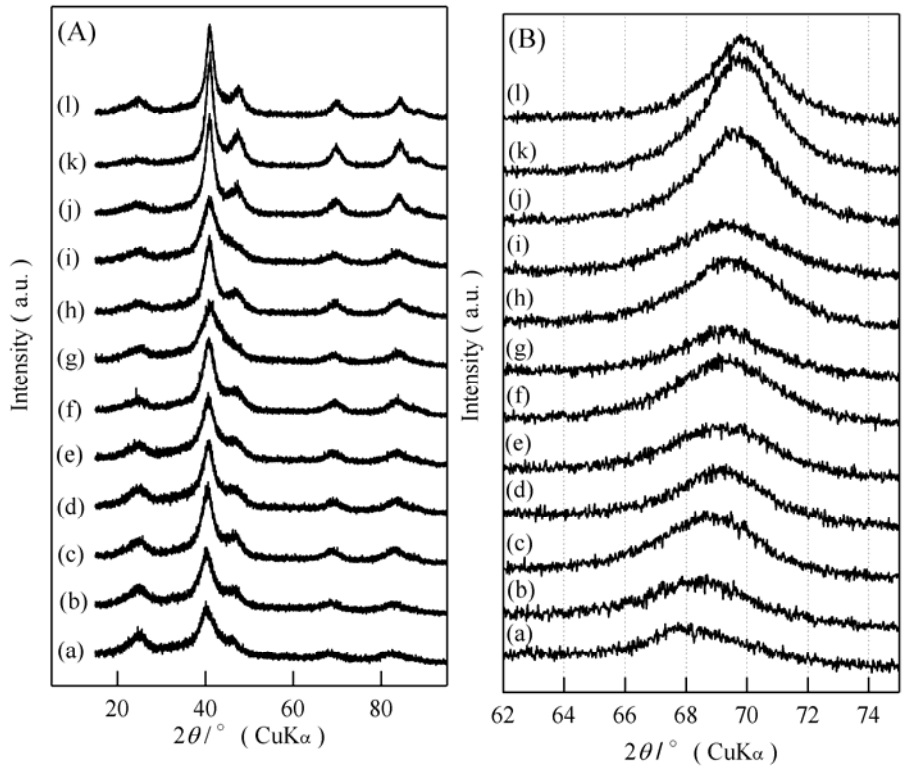

Fig. 3. The XRD patterns of PtRuRh/C catalyst prepared with different molar ratio of Pt, Ru and Rh. (A) Wide angle profile and (B) detailed measurements near the fcc 220 peak. (a) 1:1:0 (b) 1:1/2:1/2, (c) 1:1/2:1, (d) 1:1:1/2, (e) 1:1:1, (f) 1:1:2, (g) 1:2:1, (h) 1:1:3, (i) 1:2:2, (j) 1:1:4, (k) 1:1:8, (l) 0:0:1.

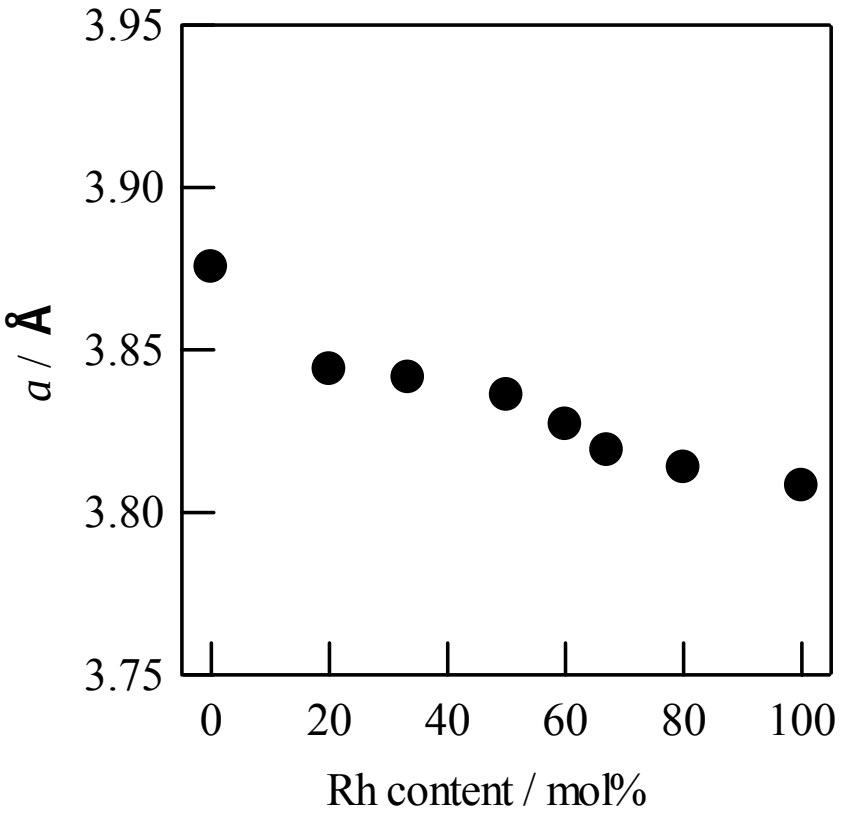

Fig. 4. The fcc lattice parameter *a* of the $Pt_1Ru_1Rh_x$/C alloy catalysts against the Rh content, where these alloy particles were assumed to be well homogeneous.

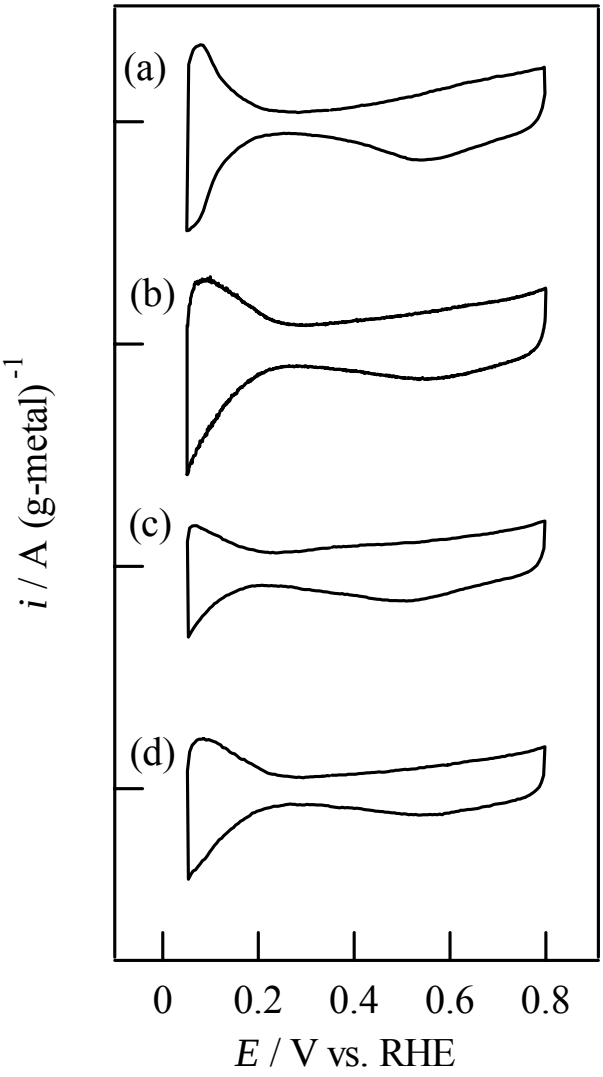

Fig. 5. Typical steady-state cyclic voltammograms of (a) $Pt_1Ru_1Rh_2/C$, (b) $Pt_2Ru_1Rh_1/C$, (c) $Pt_1Ru_2Rh_1/C$, and (d) $Pt_2Ru_1Rh_2/C$ in 0.5 M H_2SO_4 60 °C at 10 mV s^{-1}.

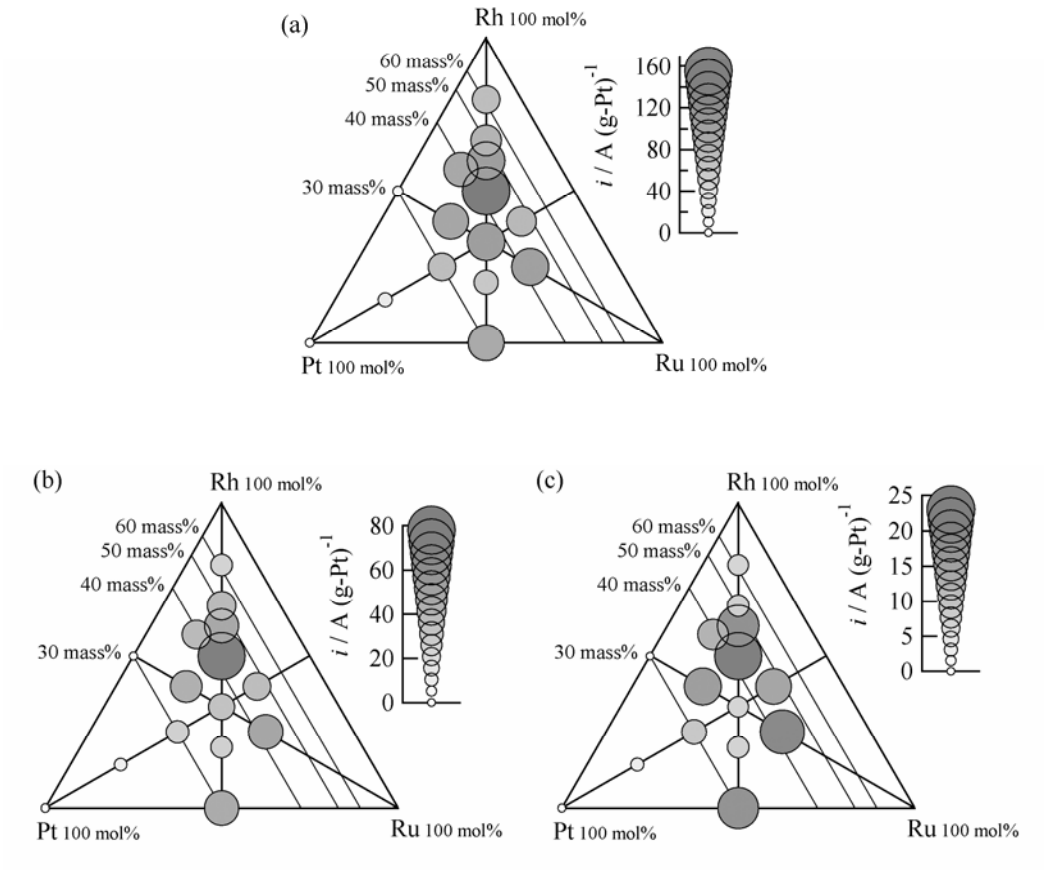

Fig. 6. The mass specific current density per unit mass of Pt measured after 30 min at (a) 0.50, (b) 0.45 and (c) 0.40 V vs. RHE in 0.5 M H_2SO_4 + 1 M CH_3OH at 60 °C.

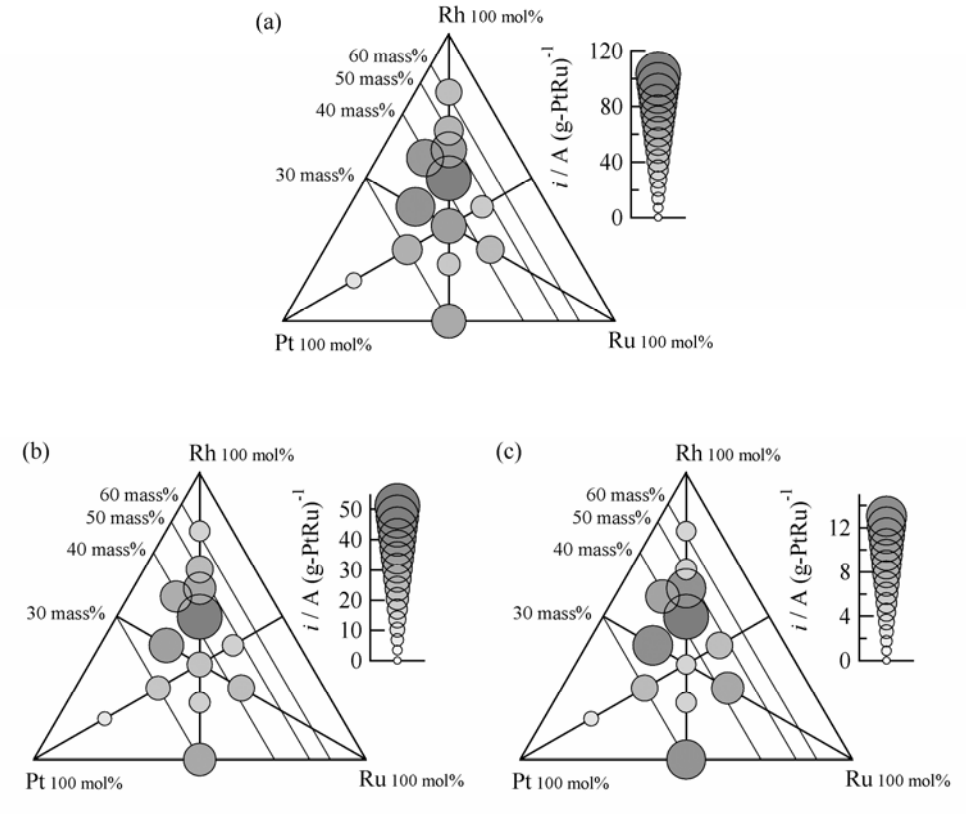

Fig. 7. The mass specific current density per unit mass of PtRu measured after 30 min at (a) 0.5, (b) 0.45 and (c) 0.4 V vs. RHE in 0.5 M H_2SO_4 + 1 M CH_3OH at 60 °C.

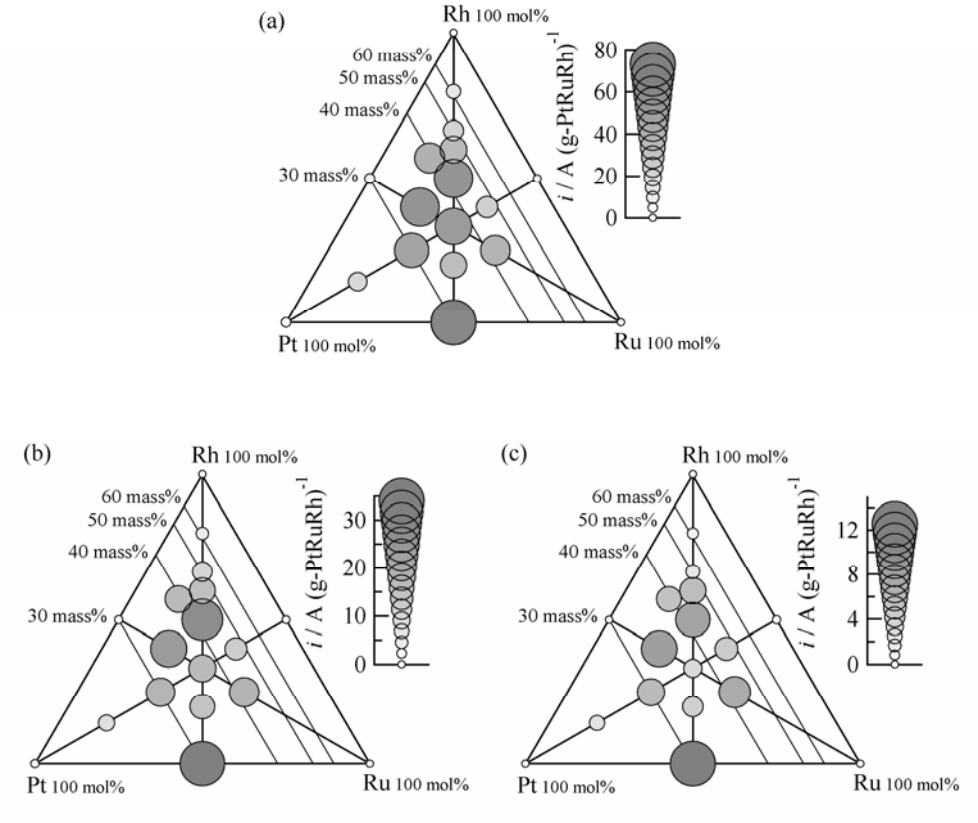

Fig. 8. The mass specific current density per unit mass of PtRuRh measured after 30 min at (a) 0.50, (b) 0.45 and (c) 0.40 V vs. RHE in 0.5 M H_2SO_4 + 1 M CH_3OH at 60 °C.

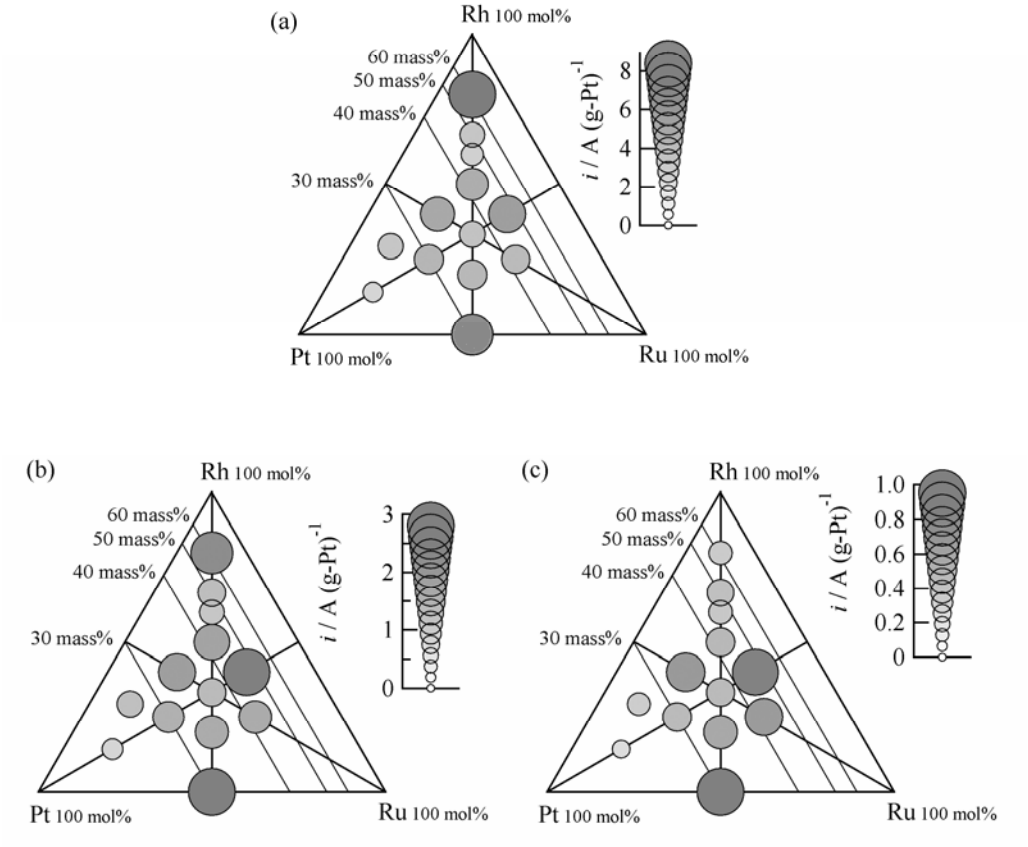

Fig. 9. The mass specific current density per unit mass of Pt measured after 30 min at (a) 0.50, (b) 0.45 and (c) 0.40 V vs. RHE in 0.5 M H_2SO_4 + 1 M CH_3OH at 25 °C.

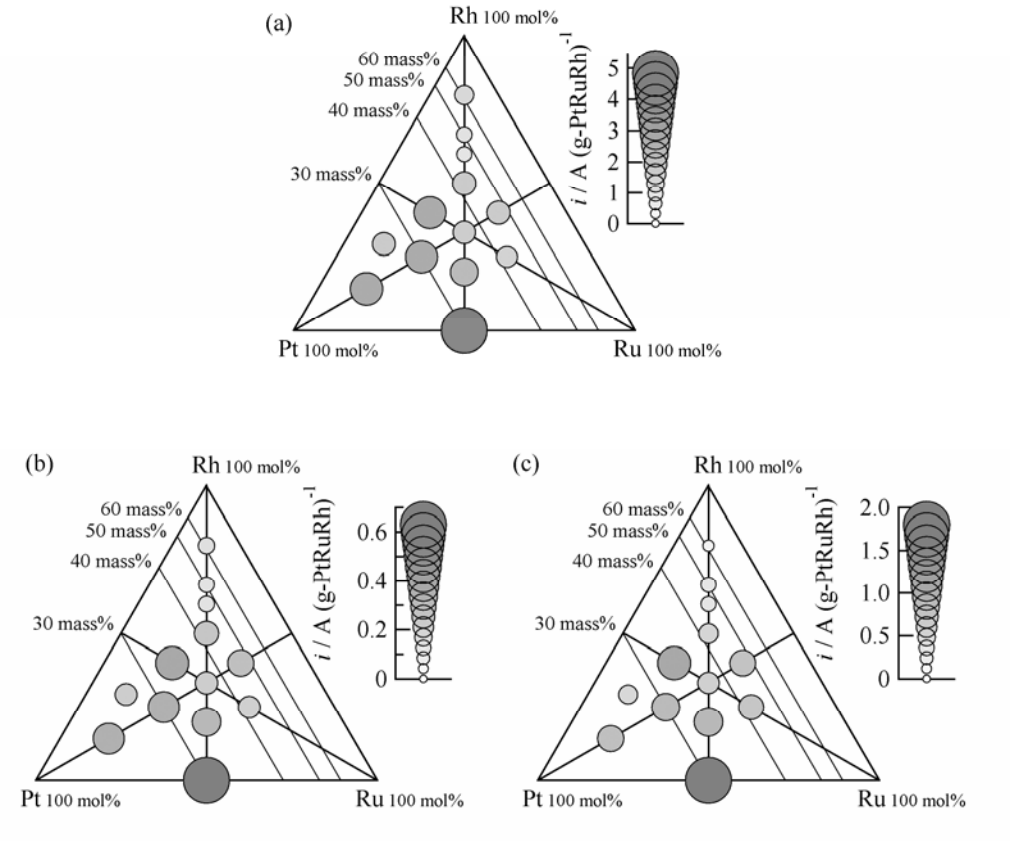

Fig. 10. The mass specific current density per unit mass of PtRuRh measured after 30 min at (a) 0.50, (b) 0.45 and (c) 0.40 V vs. RHE in 0.5 M H_2SO_4 + 1 M CH_3OH at 25 °C.